23rd ABCM International Congress of Mechanical Engineering
December 6-11, 2015, Rio de Janeiro, RJ, Brazil

SOLUTION VERIFICATION TEST BY A CFD MIXED HIGH ORDER CODE IN LAMINAR-TURUBULENT FLOW TRANSITION

Homero Ghioti da Silva
Faculdade de Ciência Integrada do Pontal, Universidade Federal de Uberlândia, Rua 20, 1600, 38304402,Ituiutaba,Minas Gerais, Brazil
ghioti@pontal.ufu.br

Abstract. *This work treats uncertainty quantifications in CFD of high order of accuracy, in the context of Verification and Validation. The work was performed into numerical solutions by one in-house code that uses mixed high-order method, composed by compact finite difference methods at 4th to 6th order of accuracy, used to the spatial derivative calculations, and Runge Kutta method of 4th order of accuracy, used to the numerical integration calculations of the Navier/Stokes equations. The code simulates the flow laminar-turbulent transition in a channel flow. The numerical error was estimated through comparisons between numerical solutions and one reference solution by the Richardson extrapolation method on numerical solution on two different mesh level. The comparisons and the estimation to numerical error were studied in a mesh convergence test. Further, an uncertainty quantification using grid convergence index (Roache's GCI) was performed. The results confirmed great estimative to the discretization erros. The estimated order of accuracy was in agreement with the formal order of accuracy of the current numerical schemes. Because of mixed high order code adopted, the interpretation of results in the mesh refinement test was hard, but, it was possible to explain the origin and contribution of each dominant estimated numerical error.*

Keywords: *Uncertainties quantification, Mixed high-order code, CFD in flow laminar-turbulent transition, Richardson extrapolation, Roache's GCI*

1. INTRODUCTION

Solution Verification Tests concern to the quantification of numerical uncertainties on the numerical results. So, what the confiability degree to the results, under confidence at 95%, is the main question involved in this research area. Solution verification should be treated in the context of (V&V) verification and validation, (Roache, 2009). This one is an important concept, composed by studies of verification tests and validation of results, both in attempt to reach good quality of numerical results from computational codes and the assurance that the problem in question was, in fact, modeled correctly. In Computational Fluid Dynamics (CFD), verification and validation are different concepts and one cannot replace the other. According to Roache (2009), verification consists in assuring that the numerical model is resolved correctly. Validation assures that the expectations of the underlying physical model agree with the experimental evidence. In other words, while the validation test involves comparisons between numerical solutions and experimental results, verification is a purely mathematical exercise, with no concern whatsoever to the adequacy of physical laws. Verification test can be divided into two categories: code verification and solution verification. They are different concepts inside of verification test. While solution verification involves the estimation (assessment) of the total numerical error (iterative, discretization and round-off), which always exists when equations are resolved numerically, code verification to evaluate the implementation of equations, boundary conditions and discretization scheme as a whole, in order to ensure the absence of programming errors.

The main goal this work was to investigate the Roache's GCI Index, coupled with Richardson extrapolation to the error estimation (Roache, 2009), as a good alternative to solution verification test in numerical results by mixed high order code.

The current solution verification test was applied into numerical solutions from a in-house mixed high order code developed to simulate the natural transition due the temporal evolution of wavepackets in a Plane Poiseuille Flow (Silva, et al., 2009). This physical problem was modeled by three-dimensional Navier-Stokes equations assuring mass conservation and solenoidal vector fields. The equations were treated on a vorticity-velocity formulation and a mixed high order scheme, from $4th$ to $6th$ order of accuracy, depending of position in the domain, equations and variables, was implemented in the code. In the current context, care should be taken to assure the formal high order of accuraccy, supposed done by theorethical numerical schemes, can be confirmed by the numerical results. (Souza et al., 2005).

According to Roache (2009), solution verification test should be performed after a code verification test, which can give reliability that the code was debugged. This is done because programming errors can affect the results and gives misleading interpretation on the uncertainty to the solutions. There are a number of ways to execute code verification, such as, comparisons between the numerical solution and an analytical solution, comparisons code to code and the Method of Manufactured Solutions (MMS), (Roache, 2009; Roy, 2005). The two-dimensional version of the cuurent code was submitted to a Verification Test using the MMS and the results can be found in (Silva et al., 2010). There, it was possible to create a manufactured solution that satisfied the boundary condition implemented in the code and able to test all routines completely, including nonlinear terms and the results gave confiability that the numerical code was free of programming errors.

One way to perform solution verification is to construct a reference solution by Richardson extrapolation using the numerical solutions on different mesh levels (Roache, 2009). In this paper, the modified three-dimensional problem with MMS was held. The numerical error was estimated from numerical solutions on different mesh levels when compared with a Richardson Extrapolation solution (obtained from them) with largest order of accuracy. So, time and spatial tests through of a grid refinement test were performed. Further, the uncertainties quantification from numerical solutions, using Grid Convergence Index (GCI), was performed. The results were studied on global and local analysis. The chosen number of mesh levels allowed to reach the assymptotic range, i.e, the refinement stage where the numerical error from approximation that result the lowerst order of accuracy takes over. The results indicated that the Roache's GCI index, coupled with Richarson exptrapolation to error estimation, remain a good alternative to quantify the numerical uncertainties from numerical solutions by mixed high order code.

The organization of the paper is as follows. Section 2 presents the formulation, the interest problem and the equations, the boundary conditions and the numerical method adopted in the present work. Further, the modified problem by MMS also was presented. Section 3 explains in detail the solution verification procedure employing Richardson Extrapolation and chosen mesh levels. Section 4 shows the mesh convergence tests performed and gives the results about estimated errors. Section 5 presents some final remarks.

2. METHODOLOGY

2.1 Formulation

The governing equations were used to incompressible three-dimensional flow. In the numerical simulations, these equations were used in a vorticity-velocity formulation. The Navier/Stokes equations were converted into transport of vorticity $\vec{\omega}$-equations

$$\frac{\partial \vec{\omega}}{\partial t} = (\vec{\omega} \cdot \nabla)\vec{u} - \vec{u} \cdot \nabla \vec{\omega} + \frac{1}{Re}\nabla^2 \vec{\omega}, \tag{1}$$

where the components of $\vec{\omega}$ are

$$\omega_x = \frac{\partial v}{\partial z} - \frac{\partial w}{\partial y}, \quad \omega_y = \frac{\partial w}{\partial x} - \frac{\partial u}{\partial z}, \quad \omega_z = \frac{\partial u}{\partial y} - \frac{\partial v}{\partial x}. \tag{2}$$

From equation (2) and using the fact that both velocity and vorticity vector fields are solenoid,

$$\nabla \cdot \vec{u} = 0, \quad \nabla \cdot \vec{\omega} = 0, \tag{3}$$

one obtains a Poisson equation for the velocity field

$$\nabla^2 \vec{u} = -\nabla \times \vec{\omega}. \tag{4}$$

The above equations were made dimensionless using U_{max}, which is the maximum velocity in the channel, and H, half the channel height. These variables produce the following dimensionless parameters:

$$x = \frac{x^*}{H}, \qquad y = \frac{y^*}{H}, \qquad z = \frac{z^*}{H}, \tag{5}$$

$$u = \frac{u^*}{U_{max}}, \qquad v = \frac{v^*}{U_{max}}, \qquad w = \frac{w^*}{U_{max}}, \tag{6}$$

$$\omega_x = {\omega_x}^* \frac{H}{U_{max}}, \qquad \omega_y = {\omega_y}^* \frac{H}{U_{max}}, \qquad \omega_z = {\omega_z}^* \frac{H}{U_{max}}, \tag{7}$$

$$t = t^* \frac{U_{max}}{H}, \tag{8}$$

where the terms with an asterisk are dimensional. The Reynolds number (Re) is $\frac{U_{max}H}{\nu}$, where ν denotes the kinematic viscosity.

In the numerical simulations, the so-called disturbance formulation was employed as it provides better accuracy. This formulation stems from the fact that the total flow is composed by a small three-dimensional disturbance and the plane Poiseuille flow. Therefore, the variables can be written as :

$$u = \bar{U} + u^{'}; \; v = v^{'}; \; w = w^{'} \tag{9}$$

$$\omega_x = \omega_x^{'}; \; \omega_y = \omega_y^{'}; \; \omega_z = \bar{\Omega}_z + \omega_z^{'}, \tag{10}$$

where $\bar{U}(y) = 2y - y^2$ is the plane Poiseuille flow and $\bar{\Omega}_z(y) = 2 - 2y$ is its spanwise vorticity. The variables $u^{'}, v^{'}$ and $w^{'}$ are the velocity disturbance components and $\omega_x^{'}$, $\omega_y^{'}$ and $\omega_z^{'}$, the vorticity disturbance components. Substituting these expressions into equations (1) and (4) the terms relative to the base flow cancel out and one obtains the vorticity transport equations for the disturbances only

$$\frac{\partial \omega_x^{'}}{\partial t} = -\frac{\partial a}{\partial y} + \frac{\partial b}{\partial z} + \frac{1}{Re}\nabla^2 \omega_x^{'} \tag{11}$$

$$\frac{\partial \omega_y^{'}}{\partial t} = \frac{\partial a}{\partial x} - \frac{\partial c}{\partial z} + \frac{1}{Re}\nabla^2 \omega_y^{'} \tag{12}$$

$$\frac{\partial \omega_z^{'}}{\partial t} = -\frac{\partial b}{\partial x} + \frac{\partial c}{\partial y} + \frac{1}{Re}\nabla^2 \omega_z^{'}; \tag{13}$$

where

$$a = v^{'}\omega_x^{'} - (\bar{U} + u^{'})\omega_y^{'}, \tag{14}$$

$$b = (\bar{U} + u^{'})\omega_z^{'} + u^{'}\bar{\Omega}_z - w^{'}\omega_x^{'}, \tag{15}$$

$$c = -v^{'}(\bar{\Omega}_z + \omega_z^{'}) + w^{'}\omega_y^{'}, \tag{16}$$

are the nonlinear quadratic terms.

With some algebraic manipulations of equations (2) to (4), the following equations for the velocity disturbance can be obtained

$$\frac{\partial^2 u^{'}}{\partial x^2} + \frac{\partial^2 u^{'}}{\partial z^2} = -\frac{\partial \omega_y^{'}}{\partial z} - \frac{\partial^2 v^{'}}{\partial x \partial y}; \tag{17}$$

$$\nabla^2 v^{'} = \frac{\partial \omega_x^{'}}{\partial z} - \frac{\partial \omega_z^{'}}{\partial x}; \tag{18}$$

$$\frac{\partial^2 w^{'}}{\partial x^2} + \frac{\partial^2 w^{'}}{\partial z^2} = \frac{\partial \omega_y^{'}}{\partial x} - \frac{\partial^2 v^{'}}{\partial y \partial z}. \tag{19}$$

The formulation has no explicit boundary conditions for vorticity at the wall. This has to be calculated from the velocity field assuring consistency and conservation of mass. More in depth discussion of the current formulation as compared with the primitive variable formulation can be found in (Fasel et al., 1980; Gatski, 1991 and Meitz and Fasel, 2000).

Temporal instability is considered. Periodic boundary conditions were adopted in both streamwise and spanwise directions (x and z). For the wall-normal direction ($y-$direction), no-slip and no-penetration ($u = v = w = 0$ at the walls) conditions were imposed. The flow geometry is presented in figure 1.

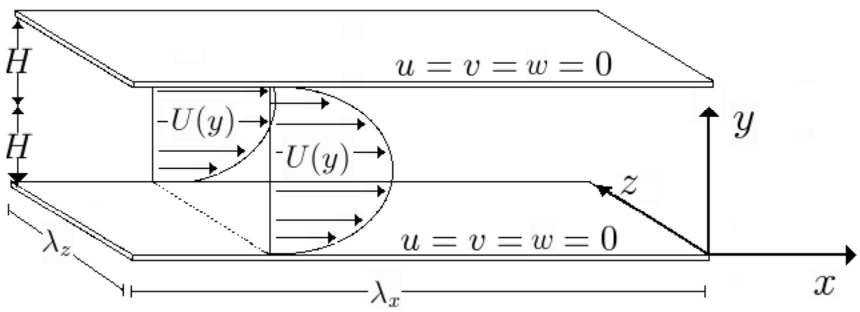

Figure 1. Schematic of flow geometry.

2.2 Numerical scheme

This formulation has been successfully in several investigations on spatial instability in boundary layers and channel flow (Fasel and Bestek, 1980). For temporal instability, where a periodic boundary condition is used in the streamwise direction, had to use an iterative procedure to solve the vorticity boundary condition at the wall. In the current work, a different approach was developed that restricted the iterative procedure to the mean flow Fourier component. Owing to this original procedure, the numerical scheme is explained here in some detail.

In the code, a pseudo-spectral method was used for the x and $z-$directions. In this method, a generic quantity s can be decomposed into Fourier modes (α_l, β_k) as

$$s(x,y,z,t) = \sum_{k=0}^{N_k}\sum_{l=0}^{N_x} S_{l,k}(y,t)e^{-i(\alpha_l x+\beta_k z)}, \tag{20}$$

where s represents the variables $u^{'}, v^{'}, w^{'}, \omega^{'}_x, \omega^{'}_y, \omega^{'}_z, a, b$ and c in physical space. $S_{l,k}$ represents the discrete Fourier components of the function s. Furthermore, $\alpha_l = \frac{2\pi l}{\lambda_x}$; $-N_x \le l \le N_x$ and $\beta_k = \frac{2\pi k}{\lambda_z}$; $-N_z \le k \le N_z$ are, respectively, the spanwise and streamwise wavenumbers; λ_x and λ_z are the wavelengths that correspond to the domain size in x and $z-$directions respectively.

Substituting the expression (20) into equations (11) to (13) and (17) to (19) one obtains

$$\frac{\partial \Omega_x^{l,k}}{\partial t} = -\frac{\partial A^{l,k}}{\partial y} - \beta_k B^{l,k} + \frac{1}{Re}{\nabla^{l,k}}^2\Omega_x^{l,k}, \tag{21}$$

$$\frac{\partial \Omega_y^{l,k}}{\partial t} = \alpha_l A^{l,k} - \beta^k C^{i.k} + \frac{1}{Re}{\nabla^{l,k}}^2\Omega_y^{l,k}, \tag{22}$$

$$\frac{\partial \Omega_z^{l,k}}{\partial t} = \beta_k B^{l,k} + \frac{\partial C^{l,k}}{\partial y} + \frac{1}{Re}{\nabla^{l,k}}^2\Omega_z^{l,k}, \tag{23}$$

$$(\alpha_l^2+\beta_k^2)U^{l,k} = \beta_k\Omega_y^{l,k} + \alpha_l\frac{\partial V^{l,k}}{\partial y}; \tag{24}$$

$${\nabla^{l,k}}^2 V^{l,k} = \beta_k\Omega_x^{l,k} + \alpha_l\Omega_z^{l,k}, \tag{25}$$

$$(\alpha_l^2+\beta_k^2)W^{l,k} = -\alpha_l\Omega_y^{l,k} + \beta_k\frac{\partial V^{l,k}}{\partial y}. \tag{26}$$

Equations (21) to (23) were used for the calculation of the vorticity in the interior of the domain, while equations (24) to (26) were used for velocity.

Also, from equations (24) to (26), and considering that Ω_y is zero at the wall, the following equations hold at the wall

$$\Omega_x^{l,k} = \frac{1}{\alpha_l^2+\beta_k^2}(-\beta_k{\nabla^{l,k}}^2V^{l,k} + \alpha_l\frac{\partial\Omega_y^{l,k}}{\partial y}), \tag{27}$$

$$\Omega_y^{l,k} = 0, \tag{28}$$

$$\Omega_z^{l,k} = \frac{1}{\alpha_l}({\nabla^{l,k}}^2V^{l,k} - \beta_k\Omega_x^{l,k}), \tag{29}$$

and were used for the calculation of the vorticity there.

Each Fourier mode (α_l, β_k) was calculated independently using equations (21) to (29). The nonlinear terms of equations (21) to (23) were obtained according to the following procedure: first, the components were transformed from Fourier space to physical space by a fast Fourier transform algorithm where the nonlinear calculations were performed. After that, the results were transformed back into the Fourier space. This procedure is often named pseudo-spectral method.

For the $y-$direction, a high-order compact finite difference scheme was used. Points in the interior of the domain were discretized by centered compact finite differences of $6th$ order of accuracy. Points at the walls and next to the wall were discretized, respectively, by asymmetric schemes of $5th$ and $6th$ order of accuracy, except for the wall vorticity calculation, which used an asymmetric $6th$ order scheme. Full details of the finite difference method used can be found in (Souza and Medeiros, 2005). For all Fourier modes, except for the zeroth mode $(0,0)$, the temporal integration was carried out with an explicit $4th$ order Runge-Kutta method of four stages (Ferziger and Peric, 1997).

For $(l = k = 0)$, equations (27) and (29) proved to be unstable and $\Omega^{0,0}$ had to be calculated from its definition, equation (2). For the mode (0,0), w has to be null due to symmetry while v is null at the wall. Therefore, $\Omega_x^{0,0}$ is also null at the wall and one can write a simple equation for $\Omega^{0,0} = (0,0,\Omega_z^{0,0})$ at the wall

$$\Omega_z^{0,0} = \frac{\partial U^{0,0}}{\partial y}. \tag{30}$$

In the equation, $\Omega_z^{0,0}$ depends on $\frac{\partial U^{0,0}}{\partial y}$. However, $U^{0,0}$ cannot be calculated using equation (24). The calculation of $\Omega_z^{0,0}$ and $U^{0,0}$ had to involve an iterative procedure described below. Moreover, to ensure stability, the zeroth mode had to be advanced in time using a combination of Runge-Kutta and Crank-Nicholson methods. The procedure is similar to that employed by Marxen (1998). However, here only the zeroth mode used the iterative procedure, and the Runge-Kutta algorithm used $4th$ order instead of 2^{nd}. The whole procedure was as follows: first, write the right hand size of the spanwise vorticity transport equation (23) as

$$\frac{\partial \Omega_z^{0,0}}{\partial t} = rhs + \frac{1}{Re}\frac{\partial^2 \Omega_z^{0,0}}{\partial y^2}, \tag{31}$$

where rhs denotes right hand side. In numerical time integrations, in general, $\Omega_z|^{it+1}$ is calculated from

$$\frac{\partial \Omega_z^{0,0}}{\partial t} = \frac{1}{\Delta t}(\Omega_z|^{it+1} - \Omega_z|^{it}), \tag{32}$$

where it is the time step. At every Runge-Kutta sub-step, the diffusive term in equation (31) was calculated from a Crank-Nicholson procedure

$$\frac{\partial^2 \Omega_z^{0,0}}{\partial y^2} = \frac{1}{2}(\frac{\partial^2 \Omega_z^{0,0}}{\partial y^2}|^{it} + \frac{\partial^2 \Omega_z^{0,0^s}}{\partial y^2}|^{it+1}), \tag{33}$$

while the other terms were calculated explicitly

$$rhs = rhs^{s-1}|^{it+1}. \tag{34}$$

In the equations, $s-1 = 0, i, ii, iii$ are the sub steps of the Runge-Kutta method. When $s-1=0$ the previous time step is assumed. The diffusive term to be used in the Crank-Nicholson algorithm was calculated using high order compact schemes

$$\mathcal{A}\frac{\partial^2 \Omega_z^{0,0}}{\partial y^2}|_{j=1,N} = \mathcal{R}\Omega_z^{0,0}|_{j=1,N}, \tag{35}$$

where N is the number of points in the grid and $\mathcal{A}$ and $\mathcal{R}$ are the coefficient matrices of the linear system that had to be solved.

Combining equations (31) to (35) one arrives at

$$(\frac{\Delta t}{2Re}\mathcal{R} - \mathcal{A})\Omega_z^{0,0^s}|_{j=1,N}^{it+1} = (\frac{\Delta t}{2Re}\mathcal{R} + \mathcal{A})\Omega_z^{0,0^s}|_{j=1,N}^{it} - \Delta t\mathcal{A}rhs^{s-1}|^{it+1}. \tag{36}$$

This equation was iterated. In order to reach convergence, the $\Omega_z^{0,0}$ values at the wall had to be underrelaxed as follows:

$$\Omega_z|^{0,0^s}{}_{j=1} = \frac{l-1}{l_{max}-1}\Omega_z{}^{0,0^s}|_{j=1}^{it+1} + \frac{l_{max}-l}{l_{max}-1}\Omega_z{}^{0,0}|_{j=1}^{it}, \tag{37}$$

$$\Omega_z|^{0,0^s}{}_{j=N} = \frac{l-1}{l_{max}-1}\Omega_z{}^{0,0^s}|_{j=N}^{it+1} + \frac{l_{max}-l}{l_{max}-1}\Omega_z{}^{0,0}|_{j=N}^{it}, \tag{38}$$

where l_{max} is the number of iterations to reach convergence. In the current work, $l_{max}=2$ was sufficient as opposed to that of (Marxen, 1998) where $l_{max}=7$. It is believe that this faster convergence was a result of using the interaction only for the zeroth mode, which does not change quickly in time. At interior points,

$$\Omega_z|^{0,0^s}{}_{j=2,N-1} = \frac{1}{2}(\Omega_z{}^{0,0^s}|_{j=2,N-1}^{it+1} + \Omega_z{}^{0,0}|_{j=2,N-1}^{it}), \tag{39}$$

was used.

Overall, the scheme can be summarized as

1. Calculate the nonlinear terms $A_{l,k}$, $B_{l,k}$ and $C_{l,k}$ in the physical domain and transform them back to the Fourier space;

2. Calculate the right-hand side of the vorticity transport equation, equations (21) to (23), excluding the wall-normal diffusion term only for mode $(0,0)$, ie., $\frac{1}{Re}\frac{\partial^2 \Omega_z^{0,0}}{\partial y^2}$;

3. Calculate a first estimate for wall-normal diffusion $\frac{1}{Re}\frac{\partial^2 \Omega_z^{0,0}}{\partial y^2}$ using compact finite differences;

4. Integrate the vorticity transport equation, equations (21) to (23), in one stage using the Runge-Kutta method of $4th-$order of accuracy. Here, all the Fourier modes should be calculated including the zeroth mode. The value of the zeroth mode is used to start the iteration described in the item 8 below;

5. Calculate the velocity component $V^{l,k}$ using equation (25);

6. Calculate the velocity components $U^{l,k}$ and $W^{l,k}$ using equations (24) and (26) respectively;

7. Calculate the wall vorticity using equations (27) to (30).

8. Calculate the wall-normal diffusion term $\frac{1}{Re}\frac{\partial^2 \Omega_z^{0,0}}{\partial y^2}$ implicitly with a Crank-Nicholson method. Since there is no boundary condition for the vorticity at the wall, the following iteration procedure is necessary:

    a) Calculate $U^{0,0}$ for all points of the domain and $\Omega_z^{0,0}$ only for the points at the walls;

    b) Underrelax the $\Omega_z^{0,0}$ values at the wall;

    c) Using the wall vorticity values as boundary conditions, calculate the new vorticity values inside the domain, using equation (36).

9. Turn back to item 1 and repeat the above calculation up to the number of time steps desired.

As the Fourier modes were calculated independently, it is not necessary that item 6 be performed before item 7.

2.3 The Modified Problem by the Method of Manufactured Solutions (MMS)

The Chosen Manufactured Solution was a three-dimensional extension that manufactured solution showed by Silva et al. (2010). The form to the streamwise and spanwise velocity components was:

$$u(x,y,z,t) = A_0 \mathrm{e}^y y(y+1-\sqrt{5})(y+1+\sqrt{5})(y-2)\mathrm{cos}(\alpha x+\beta z-\omega t), \tag{40}$$
$$w(x,y,z,t) = A_0 \beta \mathrm{e}^y y(y+1-\sqrt{5})(y+1+\sqrt{5})(y-2)\mathrm{cos}(\alpha x+\beta z-\omega t), \tag{41}$$

where A represents the wave amplitude. In the solution, the expression e^y ensures that the $y-$derivatives of any order are non-zero. This is necessary for a systematic study of order of accuracy via a mesh refinement test. Note that u satisfies the boundary conditions for the flow of interest. It is periodic in the $x-$ and $z-$directions, with a non-dimensional wavelength $\lambda_x = 2\pi/\alpha$ and $\lambda_z = 2\pi/\beta$ respectively, and satisfies the non-slip condition at the walls. ω is the time frequency number and this manufactured solution oscillates in time. It mimics a Tollmien-Schlichting wave that propagates along of plane Poiseuille flow satisfying constant amplitude. The streamwise and spanwise wavenumbers (α and β) were dimensionless by H.

Substituting the equations (40) and (41) into continuity equation, one obtains the wall-normal velocity component (v) as:

$$v(x,y,z,t) \;=\; A\sin(\alpha x+\beta z-\omega t)\mathrm{e}^y y^2(\beta^2 y^2 - 4\beta^2 y + 4\beta^2 + \alpha y^2 - 4\alpha y + 4\alpha). \tag{42}$$

For v to satisfy the impermeability boundary condition, the factors $(y+1-\sqrt{5})$ and $(y+1+\sqrt{5})$ in u and w were necessary.

The vorticity components were obtained from its definition, equation (2), as:

$$\begin{aligned} \omega_x(x,y,z,t) &= A\beta \mathrm{e}^y \mathrm{cos}(\alpha x+\beta z-\omega t)(-y^4+8y^2-8-4y^3+\beta^2 y^4 \\ &\quad -4\beta^2 y^3 + 4\beta^2 y^2 + y^4\alpha - 4y^3\alpha + 4\alpha y^2 + 8y), \end{aligned} \tag{43}$$
$$\begin{aligned} \omega_y(x,y,z,t) &= -A\mathrm{e}^y y\sin(\alpha x+\beta z-\omega t)\beta(y^3\alpha - 8\alpha y + 8\alpha - y^3 \\ &\quad +8y-8), \end{aligned} \tag{44}$$
$$\begin{aligned} \omega_z(x,y,z,t) &= -A\mathrm{e}^y \mathrm{cos}(\alpha x+\beta z-\omega t)(\alpha y^4\beta^2 - 4\alpha y^3\beta^2 + 4\alpha y^2\beta^2 \\ &\quad +\alpha^2 y^4 - 4\alpha^2 y^3 + 4\alpha^2 y^2 + 8y - y^4 + 8y^2 - 8 - 4y^3). \end{aligned} \tag{45}$$

Figure 2 shows $u-$ velocity and ω_y-vorticity components for $\alpha = \beta = Re = 1$ (Reynolds number based on half the channel height and on the velocity at the centerline of the channel, equations (5) and (6). Setting the Reynolds number to 1 ensures that the convective and diffusive terms are of similar order of magnitude. This helps to avoid hiding of programming errors (Roache, 2009; Silva et al., 2010).

The manufactured solution described above is the analytical solution of the following fictitious problem:

$$\frac{\partial \omega_x}{\partial t} \;=\; -\frac{\partial a}{\partial y} + \frac{\partial b}{\partial z} + \frac{1}{Re}\nabla^2\omega_x + F_x(x,y,z,t) \tag{46}$$
$$\frac{\partial \omega_y}{\partial t} \;=\; -\frac{\partial a}{\partial x} + \frac{\partial c}{\partial z} + \frac{1}{Re}\nabla^2\omega_y + F_y(x,y,z,t) \tag{47}$$
$$\frac{\partial \omega_z}{\partial t} \;=\; -\frac{\partial b}{\partial x} + \frac{\partial c}{\partial y} + \frac{1}{Re}\nabla^2\omega_z + F_z(x,y,z,t); \tag{48}$$

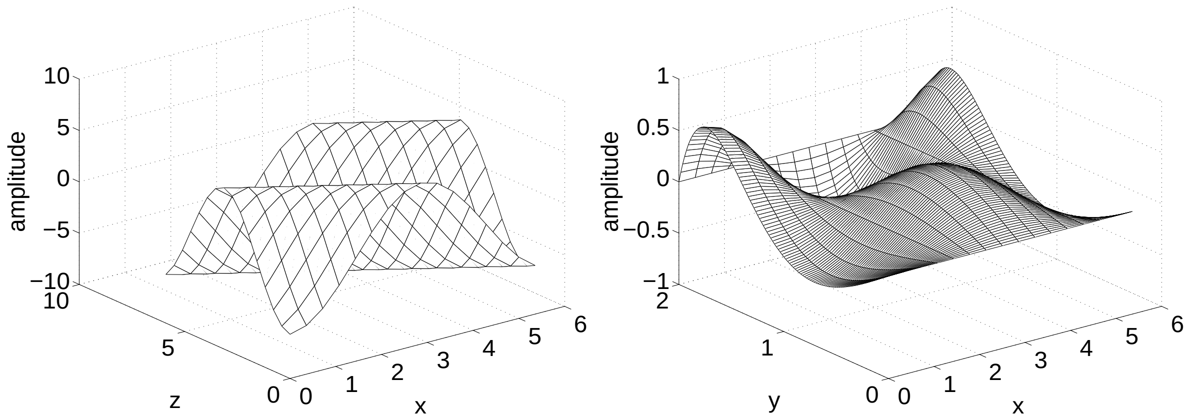

Figure 2. $u-$ velocity and ω_y-vorticity components showed on the $z = 0$ plane fixed the position $y = 1.85H$.

where F_x, F_y and F_z indicate the Forcing Terms generated from application at manufactured solution on the equations (11) to (13). The forcing terms can be found in (Silva, 2008).

Figure 3 illustrates the term F_y on the $z = 0$ plane at fixed point $y = 1.85H$. To avoid algebraic errors, a software for symbolic manipulation (Maple-6) was used to obtain the F source term components.

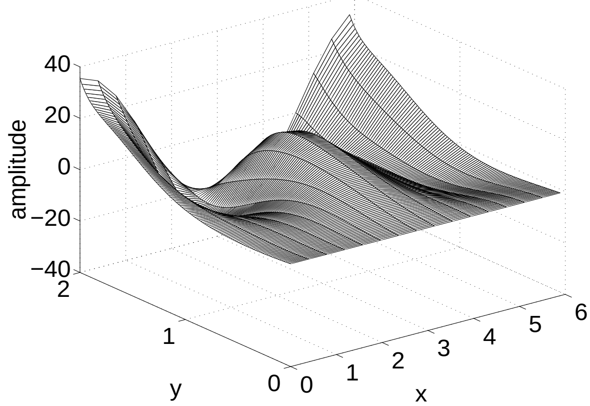

Figure 3. F_y component of the forcing term F on the $z = 0$ plane fixed the position $y = 1.85H$.

3. ERROR ESTIMATIONS AND RICHARDSON EXTRAPOLATION

According to Roache (2009) error estimation can be done generating a Richardson polynomial by extrapoling from two numerical solutions on different mesh levels. Richardson Extrapolation can be generated from solutions on a fine mesh (namely h1) and a coarse mesh (namely h2). The ration $r = h2/h1$ shouldn't necessarily be the number two, i.e., doubling the number of mesh points. This work used the non-integer refinement $r = 1.125$ to generate the Richardson Extrapolation expression. It can be good practice when results using very fine meshes turn hard. Roache (2009) indicates some examples of applications where the use of doubling number of points on the meshes in a refinement test can be hard. This fact repeats too in the numerical simulations to the natural transition, mainly because of high computational cost to generate results on very fine meshes and influence of round-off errors.

Richardson Extrapolation works as follow. Supposing that the dominant error from the numerical solutions is $5th-$order of accuracy, the discretization error equations to the two different meshes $h1$ and $h2$ can be written as:

$$f_1 = f_{exact} + g_6 h1^6 + \mathcal{O}(h1^7); \quad (49)$$
$$f_2 = f_{exact} + g_6 h2^6 + \mathcal{O}(h2^7); \quad (50)$$

Neglecting the higher-order terms, these two equations can be solved for f_{exact} as

$$f_{exact} \sim f_1 + \frac{f_1 - f_2}{r^6 - 1}. \quad (51)$$

Richardson (1910) showed that expression is generally of one order larger than that f_1, in this case, the Richardson Extrapolation satisfies $6th-$order of accuracy. The expression (51) follows as one correction to the most refined solution f_1, therefore, a grid refinement test can be performed to estimate the order of accuracy of the results. Important to note that Roy (2003) had emphasized that Richardson extrapolation relies on the assumption that the solutions are asymptotic (i.e., the observed order of accuracy matches the formal order). In other words, only when the asymptotic range was reached in a grid refinement test can be possible to observe the convergence order of the results. Furthermore, Richardson Extrapolation has a dispersive nature (Roache, 2009) and, because of this, it shouldn't be a satisfactory representation to the solution of the interest problem. This fact allows only the use of Richardson Extrapolation as error estimator in a calculation verification approach.

4. RESULTS

In this work, the estimation errors using Richardson Extrapolation could be composed by results to the modified problem, subsection (2.3), into two different situations, namely steady and transient states. Therefore, it was possible to estimate the numerical errors from spatial discretization (when steady state was assumed) and the influence of temporal errors from the Runge-Kutta methods, when the simulations to a long dimensionless time were performed. Different order of accuracy was identified to different positions on the mesh, equations and variables. Therefore, it was necessary to perform the analysis of results using Richardson Extrapolation satisfying $4th-$order of accuracy (case when the manufactured solution was transient), $5th$ and $6th-$order of accuracy (when the manufactured solution was steady).

Both global and local spatial discretization errors were investigated. The discretization error was measured as the relative absolute valor:

$$E_m = \frac{|f_k - RE|}{RE} \times 100 \tag{52}$$

where f_k was the numerical solution on the mesh hk and RE was the Richardson Extrapolation. The global discretization error was examined by employing maximum and mean discrete norms, namely,

$$L_1(E_m) = (\sum_{m=1}^{N} E_m)/N \tag{53}$$

$$L_\infty(E_m) = max(E_m); \tag{54}$$

where N indicates the number of points. The local spatial discretization error was investigated at different points of the domain.

The mesh convergence test was performed only in the $y-$direction using the $y-$refinement showed in table 1. This is because in both $x-$ and $z-$directions the numerical error have only round-off error. Since the manufactured solution had a single cosine mode in both $x-$ and $z-$directions respectively, the x and $z-$truncation errors were null. The number of points in both $x-$ and $z-$directions was fixed at 8, dx and dz where done by $2\pi/(\alpha N_x) = 0.19635\alpha$. and $2\pi/(\beta N_z) = 0.19635\beta$ respectively. To avoid the influence of round off error on the results, it was necessary to perform the calculations using quadruple precision.

Table 1. Meshes used in the grid refinement test. N_y indicates the number of points in the direction y.

mesh	N_y	$\Delta y = 2/(N_y - 1)$	$hi/h1$
h1	451	0.00444	1.00000
h2	401	0.00500	1.12500
h3	351	0.00571	1.28571
h4	301	0.00666	1.50000
h5	251	0.00800	1.80000
h6	201	0.01000	2.25000
h7	151	0.01333	3.00000
h8	101	0.02000	4.50000
h9	51	0.04000	9.00000

4.1 Tests on the Steady State Solutions

The test was performed using the meshes showed by table 1, satisfying $\omega = 0$, a step time $dt = 10^{-6}$. In general only 160 timesteps was simulated to assure that time discretization errors was negligible.

Global analysis

Figure 4 shows the numerical solution to the $v-$velocity and ω_z-vorticity using the mesh $h1$ and the Richardson Extrapolation as a correction from it. Note a good approximation between the results.

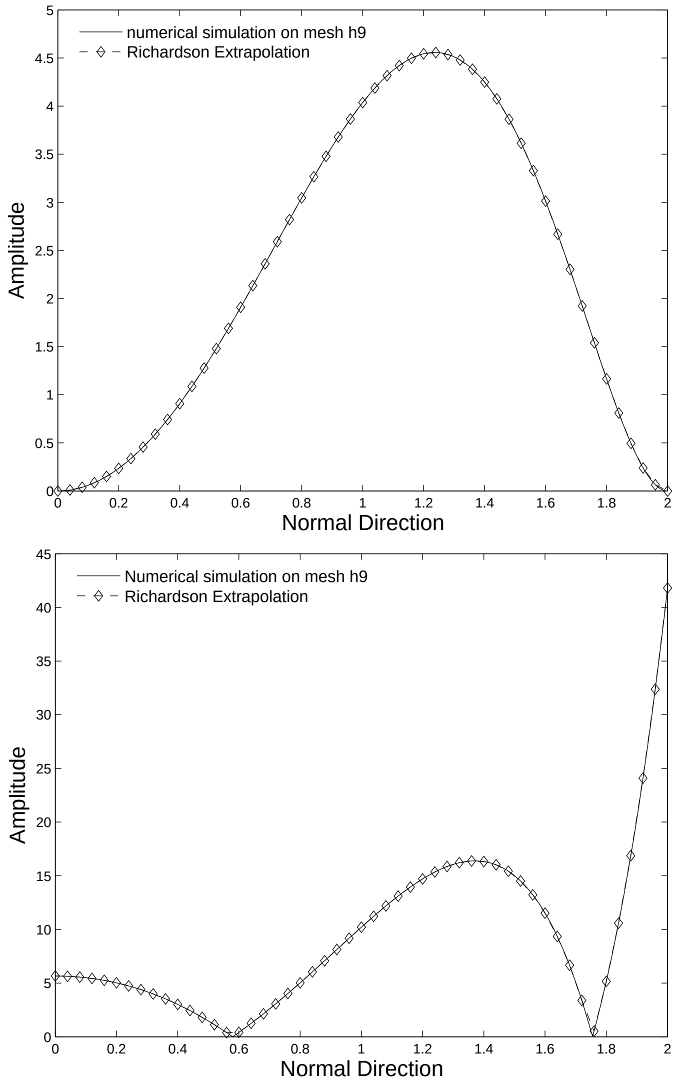

Figure 4. Numerical Simulation on the mesh $h9$, results recorded along normal direction (y) fixing the coordinates $x = 4dx$ and $z = 5dz$. **a)** $v-$velocity and **b)** ω_z-vorticity.

Figure 5 shows the behavior of the global and local discretization error for $v-$velocity component and ω_z-vorticity component when compared with Richardson Extrapolation.

The results were plotted in a logarithmic scale. It was showed results only to the $v-$velocity and ω_z-vorticity because the results for others variables presented same behavior. Both norms L_1 and L_∞ were used. The local error was recorded from the point $y = 1$. Note that $6th$ order of accuracy was observed to v, when both global and local error were calculated. Such result was clear only when finer meshes were used. In fact, it can be that the asymptotic range for this case was reached only after the adopted meshes from $h6$ to $h9$. The Figure 5 shows $5th-$order of accuracy to ω_z when global errors was calculated, and $6th-$order of accuracy when local error was calculated. One explanation to different orders of accuracy when calculated of different manners gives in fact from the dominant error of $5th-$order of accuracy from the wall vorticity calculations. As showed in subsection (2.2), the vorticity calculation was performed using mixed order on different mesh positions. In fact, while $5th-$order of accuracy was used to the wall vorticity calculation, one $6th-$order of accuracy the vorticity calculations at interior of domain was adopted. So, because of the error by wall vorticity calculation was localized and the problem was steady state, nothing contamination was recorded from wall to interior at domain to the vorticity calculations. This result is explained with details in (Silva, 2008; Silva et al., 2010). Importante to note that the results confirm those results presented by Silva et al. (2010), which involved the same equations.

Local analysis

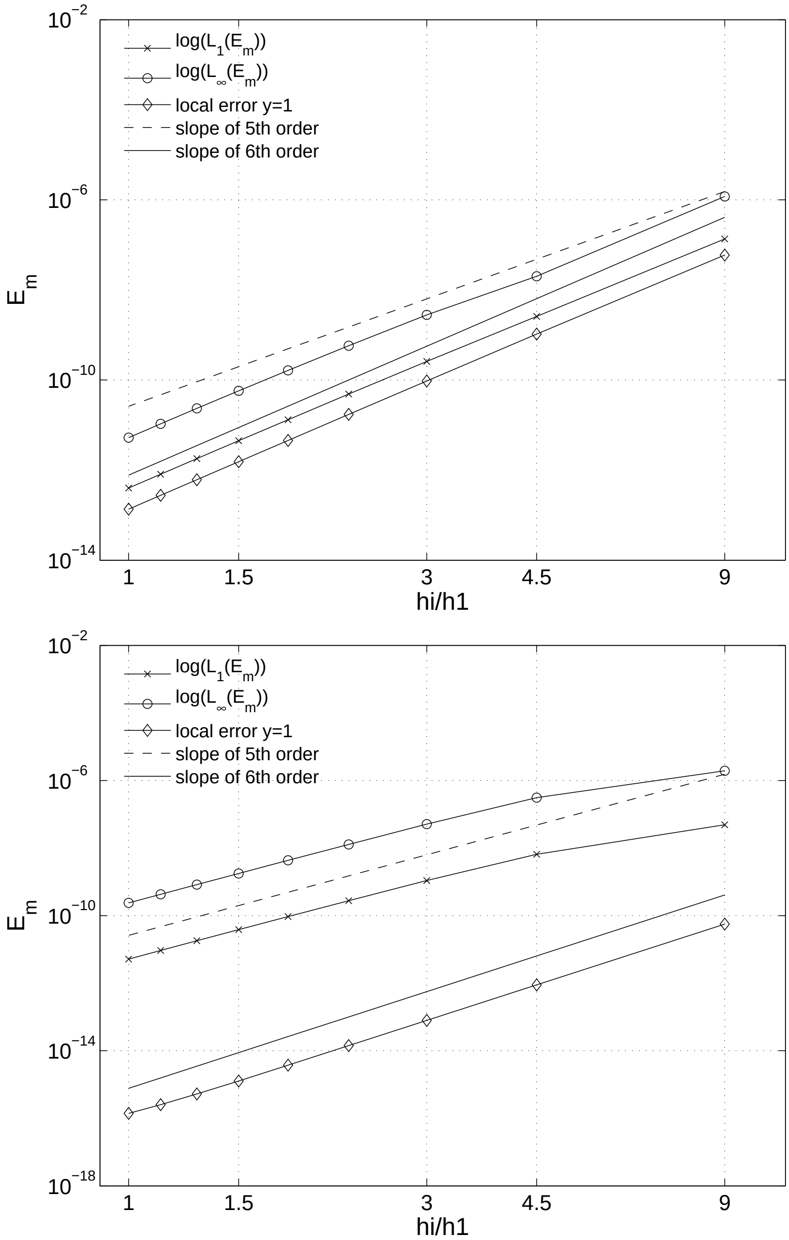

Figure 5. Estimation of the global and local discretization error E_m for the velocity and vorticity. **a)** $v-$velocity and **b)** ω_z-vorticity.

4.2 Tests on Transient State Solutions

In the proposal to estimate the convergence of errors generated by time discretization, this subsection presents error estimative to numerical solutions when the modified problem with a transient manufactured solution was adopted. Because of stability conditions to the numerical problem in question, waves amplitude set to $A = 1$ and Reynold Number set to 1, as in subsection 4.1 could not be used. In fact, to a time analysis, the temporal discretization should be dominant portion in the numerical error. Such an alternative, it was used same parameters from the temporal evolution of Tolmien-Schilichting waves in plane Poiseuille flow (Silva, 2008). This is in according to the future proposal, where error estimatives to the numerical simulation of physical problem in question will be done using the present approach.

To the manufactured solution to mimics a Tolmien Schilichting wave evolving along the Poiseuille Flow, the constant amplitude $A = 10^{-3}$ and the Reynolds Number set to 8000 were adopted. It was chosen the mesh $h2$ showed in table 1 and performed numerical simulations using timestep set to $dt = 5 \times 10^{-2},\ 1.25 \times 10^{-2},\ 0.625 \times 10^{-2},\ 3.125 \times 10^{-3}$ and $1,5625 \times 10^{-3}$. The dimensionaless time reached was $t = 8$. Therefore, the results were recorded and compared with Richardson Extrapolation when the number of timesteps was $160, 320, 640, 1280, 2560$ and 5120 respectively. According to the formal order of accuracy to the Runge-Kutta Schemes, which was $4th$, the chosen Richardson Extrapolation used to comparisons in this subsection was a correction to the numerical solution to the mesh $h2$, but satisfying $5th$ order of accuracy.

Figure 6 shows the behavior of the global and local discretization error for $v-$velocity component and ω_z-vorticity component when compared with Richardson Extrapolation.

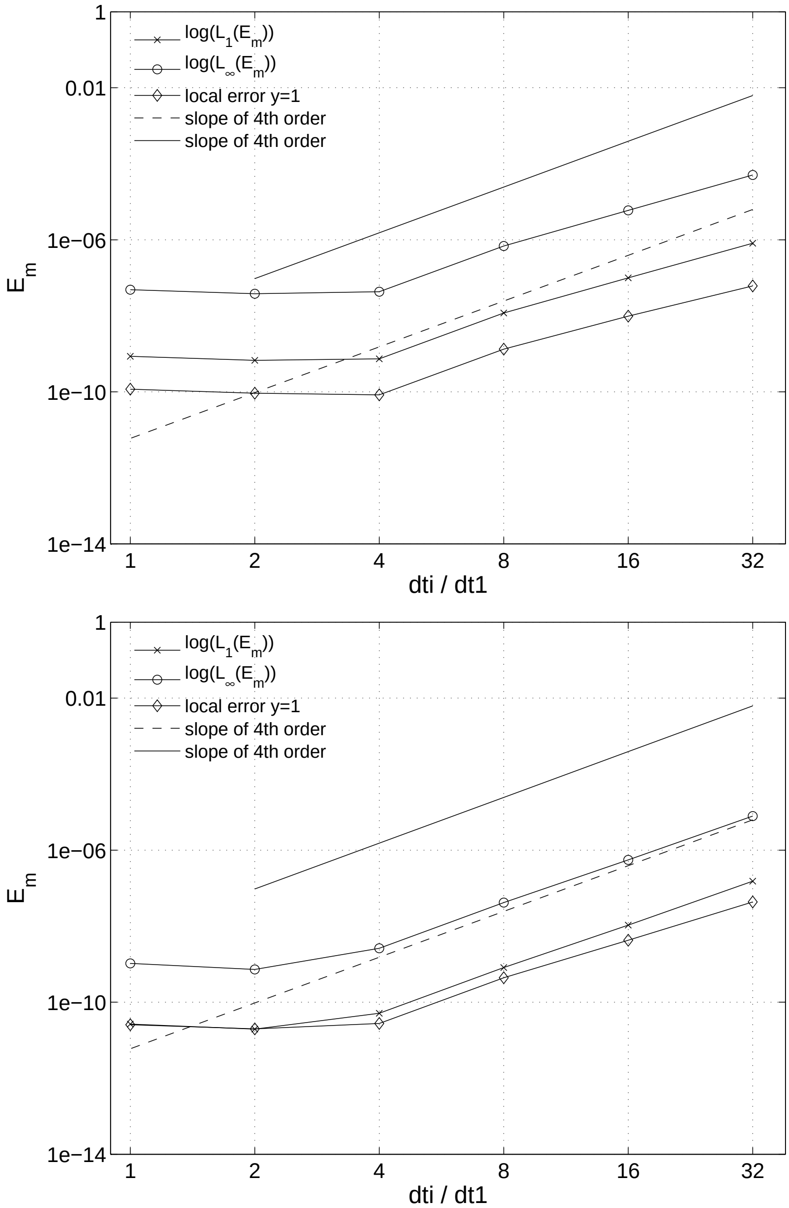

Figure 6. Estimation of the global and local discretization error E_m for the velocity and vorticity. **a)** $v-$velocity and **b)** ω_z-vorticity.

The results pointed to $4th$ order of accuracy to both $v-$velocity and ω_z-vorticity. However, when small dt was used, it became clear an error platband mainly to the $v-$velocity calculations. In fact, this error from the spatial discretization along of $y-$direction, and in attempt to turn it small, can choose a more refinement mesh in the $y-$direction, for example, the mesh $h1$. This fact was not necessary to this application and because of this it wasn't used here. Interesting that this range of timestep contains the optimal timestep used to the numerical simulation of natural transition in Plane Poiseuille Flow (Silva, 2008), when the parameters cited above were adopted. This fact can help to the estimation of errors and uncertainty analysis to the realistic problem modeled by equations 46 to 48 after erased those forcing terms.

5. FINAL REMARKS

Activites of uncertainties quantification, using the Roache's GCI index, on numerical solutions by mixed high order code, were presented in this work. First, errors estimation were performed comparing the numerical solutions with one more accuracy polinomial obtained through of Richardson Extrapolation application. Thereafter, the order of accuracy of the results was estimated in a systematic grid refinement test. Different level meshes, not-doubling points number, was adopted here, but it was possible to choose levels mesh that allows to reach the asymptotic range (Roy, 2005). The error analysis was performed adopting global norms, mean and maximum error, and local errors, choosing diferents points along of domain and stimating the absolute error in these mesh points. The Roache's GCI index, assuring an incertainties lower than five percent, was done. (Roache,2009).

The current numerical code simulates the temporal evolution of wavepackets (three-dimentional Tolmien-Schillichting waves covering differents amplitudes, wavenumbers and frequenties) in a plane Poiseuille flow, attempting to the flow transition at laminar to turbulent. The adopted numerical scheme coupled mixed high-order methods, from $4th$ to $6th$ order of accuracy, which depended of the discretized equations and position of domain. The equations and numerical scheme used in this work is an three-dimensional extension that presented in (Silva et al., 2010), where a code verification test using the Method of Manufactured Solution (MMS) was performed and the order of accuracy of results was obtained. So, the current problem, modified by the use of Method of Manufactured Solution (MMS), was simulated into three-dimensional version.

The test were composed by different stractegies, separately done, in the attempting to reach several contributions of the discretization error. First, one very small timestep short simulated time was adopted, which allowed the error estimation from the numerical solutions in a steady state. In this situation, the spatial discretization error was dominant. Second, the reverse situation was adopted, i e., one very spatially refined mesh was adopted using a timestep and time simulated like a transient situation. Although the stability condition to the methods may turn hard the choose to the time step, still it was possible to perform some verification exercise, satisfying the stability condition. In this situation the temporal discretization error was dominant.

The results confirmmed great estimative to the discretization erros. The estimated order of accuracy was in agreement with the formal order of accuracy of the current numerical schemes. In fact, the formal $5th$ and $6th$ orders of accuracy from adopted numerical scheme to the steady state, while $4th$ order of accuracy in the numerical solutions to the transient state were estimated in the current numerical solutions. Because of mixed high order code adopted, the interpretation of results in the mesh refinement test can be hard, but, in the current work, it was possible to explain the origin and contribution of each dominant stimated numerical error. Therefore, the uncertainties quantification using Roache's GCI Index could be performed with the assurance that the results were effetive.

Numerical solutions by mixed high order code have practical interest by, for example, in the laminar-turbulent flow transition, aeroacustic, aerodinamic, and others. In the situations involving geometry without discontinuities, or other complexies that have influence on the order of accuracy of the results, the Roache's GCI index, coupled with Richarson exptrapolation to error stimation, remain a good alternative to quantify the numerical uncertainties from numerical solutions by mixed high order code.

6. ACKNOWLEDGEMENTS

The authors acknowledge the FAPESP (Fundação de Amparo à Pesquisa do Estado de São Paulo), CNPq (Conselho Nacional de Desenvolvimento Científico e Tecnológico), FAPEMIG (Fundação de Amparo à Pesquisa do Estado de Minas Gerais) and UFU (University of Uberlandia) by the financial support of this research.

7. REFERENCES

Fasel, H. and Bestek, H., 1980. Investigation of Nonlinear, Spatial Disturbance Amplification in Plane Poiseuille Flow. *in Proc. Conf. on New Approaches and Concepts in Turbulence* New York.

Ferziger J. H. and Peric M., 1997. Computational Methods for Fluid Dynamics. *Springer-Verlag* Berlim, Germany.

Gatski, T. B., 1991. Review of Incompressible Fluid Flow Computations Using the Vorticity-Velocity Formulation. *Applied Numerical Mathematics* v.7, p.227-239.

Maplesoft, Developer of Advanced Mathematical and Analytical Software. *http://www.maplesoft.com/products/maple.*

Marxen O., 1998. Temporal Direct Numerical Simulation of a Flat Plate Boundary Layer, Diplomarbeit. *University of Arizona* Arizona-USA.

Meitz, H. L. and Fasel, H., 2000. A Compact-Difference Scheme for the Navier-Stokes Equations in Vorticity-Velocity Formulation. *Journal of Computational Physics* v.157, p.371-403.

Richardson L. F., 1910. The approximate arithmetical solution by finite differences of physical problems involving differential equations with an application to the stresses in a masonry dam. *Trans. Royal Society London* Ser. A 210, 307-357.

Roache P., 2009. Fundamentals of Verifcation and Validation. *Hermosa Publisher* New Mexico.

Roy C. J., 2003. Grid convergence analysis for mixed-order numerical schemes. *AIAA Journal* v.41, p.595-904.

Roy C. J, 2005. Review of code and solution verification procedures for computational simulation. *Journal of Computational Physics* v.205, p.131-156.

Roy C. J, 2009. On the generation of exact solutions for evaluating numerical schemes and estimating discretization error

Journal of Computational Physics v. 228, p.1790-1802.

Silva H. G., 2008. *Regime Não Linear de Trens de Ondas Modulados na Direção Transversal em um Escoamento de Poiseuille Plano*. PhD Thesis. Universidade de São Paulo, Brazil.

Silva, H. G., Germanos, R. A. C., Medeiros, M. A. F., 2009. Nonlinear Interaction Between Wavepackets in Plane Poiseuille Flow. *In: Seventh IUTAM Symposium on Laminar-Turbulent Transition, Stockholm. IUTAM - Seventh IUTAM Symposium on Laminar-Turbulent Transition* v. 18. p. 577-580.

Silva H. G., Souza L. F., Medeiros M. A. F., 2010. Verification of a Mixed High-Order Accurate DNS Code for Laminar Turbulent Transition by the Method of Manufactured Solutions. *Int. J. Num. Meth. Fluids* v.64, p.336-354.

Souza L. F., Mendonça M. T., Medeiros M. A. F.,2005. The advantages of using high-order finite-differences schemes in laminar-turbulent transition studies. *Int. J. Num. Meth. Fluids* v.48, p.565-582.

8. RESPONSIBILITY NOTICE

The author is the only responsible for the printed material included in this paper.